Numerical and analytical study on initial stiffness of corrugated steel plate shear walls in modular construction

En-Feng Deng [1a], Liang Zong [*2] and Yang Ding [2b]

[1] *School of Civil Engineering, Zhengzhou University, 100 Kexue Road, Zhengzhou, China*
[2] *School of Civil Engineering, Tianjin University / Key Laboratory of Coast Civil Structure Safety (Tianjin University),*
Ministry of Education, 92 Weijin Road, Tianjin, China

Abstract. Modular construction has been increasingly used for mid-to-high rise buildings attributable to the high construction speed, improved quality and low environmental pollution. The individual and repetitive room-sized module unit is usually fully finished in the factory and installed on-site to constitute an integrated construction. However, there is a lack of design guidance on modular structures. This paper mainly focuses on the evaluation of the initial stiffness of corrugated steel plate shears walls (CSPSWs) in container-like modular construction. A finite element model was firstly developed and verified against the existing cyclic tests. The theoretical formulas predicting the initial stiffness of CSPSWs were then derived. The accuracy of the theoretical formulas was verified by the related numerical and test results. Furthermore, parametric analysis was conducted and the influence of the geometrical parameters on the initial stiffness of CSPSWs was discussed and evaluated in detail. The present study provides practical design formulas and recommendations for CSPSWs in modular construction, which are useful to broaden the application of modular construction in high-rise buildings and seismic area.

Keywords: modular steel construction; corrugated steel plate; initial stiffness; finite element analysis; theoretical deviation; design recommendation

1. Introduction

Modular construction provides an excellent alternative for conventional on-site buildings with a great proportion of the building to be prefabricated in the factory. The room-sized modules are pre-made and finished, which permits the building to be put into use as soon as possible with the individual module unit to be connected with each other on site (Kim and Lee 2014, Park *et al.* 2016). Due to its high efficiency in construction, reduced environmental pollution, improved quality and low energy consumption, modular construction has received a considerable attention since the early 20th century across the construction industry (Lawson *et al.* 2014, Deng *et al.* 2017, 2018a, b). The advantages of the potential construction method can be more obvious when they are adopted for buildings with repetitive units, such as school, hospital, hotel and so on, such as the 12-story residential building in Korean (Park and Ock 2015) and Atlantic Yards B2 projects in New York (Farnsworth 2014).

Module units are conventionally made of steel, precast concrete, timber, etc, among which steel frameworks have been proven to be idealized structural form due to their lightness for transportation and convenience of connecting

by bolting. For example, container-like modules have been widely utilized for construction, making the full use of their superiority in lifting and disassembly, as illustrated in Fig. 1. The module unit will be decorated with light partition walls in the factory to provide good acoustic and thermal insulation for residential construction. The corrugated steel plate is widely used as surface enclosures of the module units and the web of steel beam to improve the shear strength (Luo and Edlund 1996, Barakat and Leblouba 2018). In urban areas, extensive demand exists in mid-to-high rise construction because of the limited space. The corrugated steel plate will serve as the lateral load–resisting component of the structure under lateral force, such as earthquake and wind (Zuo and Zha 2017, Ding *et al.* 2017). Consequently, it is crucial to investigate the lateral performance and design method of the enclosed corrugated steel plate. Initial stiffness is the most important lateral performance of the corrugated steel plate shear walls (CSPSWs) and steel plate shear walls (SPSWs), which determine the dynamic characteristics of the structure (Yu and Chen 2018, Bagherinejad and Haghollahi 2018). However, there is a lack of sufficient understanding and design guidance of CSPSWs.

Tong and Guo (2015) provided the elastic buckling resistance and shear capacity of stiffened CSPSWs through numerical investigation. Emami *et al.* (2013) conducted the cyclic tests on trapezoidally corrugated steel shear walls, indicating the better seismic performance than unstiffened steel plate shear walls (SPSWs) including higher initial stiffness, better energy dissipation capacity and improved

---

∗Corresponding author, Associate Professor,
  E-mail: zongliang@tju.edu.cn
[a] Ph.D., Lecturer, E-mail: dengenfeng@zzu.edu.cn
[b] Ph.D., Professor, E-mail: dingyang@tju.edu.cn

Fig. 1 CSPSW in modular construction

Table 1 The geometry and material properties of the specimens (Ding *et al*. 2018)

Type	Section (mm)	t^* (mm)	E^* (GPa)	f_y^* (MPa)	f_u^* (MPa)
Corrugated steel plate	Specimens CSPSW-1, CSPSW-2 and CSPSW-3	1.6 Specimens CSPSW-1, CSPSW-3 and CSPSW-4	195	388	511
	Specimen CSPSW-4	2.0 Specimen CSPSW-2	201	301	432
Frame beam/ Frame column	□150×100×6	6.0	195	394	504

*t: thickness of the steel plate; *E: elastic modulus; *f_y: yield strength; *f_u: ultimate tensile strength

buckling stability. Qiu *et al.* (2018) compared the seismic performance between SPSWs and CSPSWs. It was found that the lateral load-resisting mechanism between SPSWs and CSPSWs were different and the corrugation configuration has much influence on the seismic performance of CSPSWs. The numerical simulation conducted by Giriunas *et al.* (2012) showed that the surface corrugated steel plates were crucial lateral load–resisting components in containers. Farzampour *et al.* (2015) investigated the influence of openings on the shear capacity of CSPSWs and the reasonable location of the opening was suggested. Despite the extensive numerical and experimental study focused on the lateral performance of CSPSWs, there is limited available research on design criteria of CSPSWs, especially on the prediction of initial stiffness of CSPSWs.

This paper focuses on the initial stiffness of CSPSWs. A 3D elaborated finite element (FE) model was firstly established and validated against the tests conducted by Ding *et al.* (2018). Followed, the theoretical formulas were derived to determine the initial stiffness of CSPSWs. The accuracy of the theoretical formulas were validated by the related test and numerical results. Finally, parametric analysis was conducted and the influence of the length, height, thickness and crest height of the infill corrugated steel panel on the initial stiffness of CSPSWs was revealed. The present study extends the studies and provides useful calculation method on the initial stiffness of CSPSWs,

leading to more prevalent application of modular construction in high-rise buildings.

2. Finite element modelling

2.1 Finite element model

General purpose finite element (FE) software ABAQUS package (Version 6.13) (2013) was used to establish the FE model. The numerical results were verified by the cyclic tests conducted by Ding *et al.* (2018). The schematic view of the test setup was shown in Fig. 2(a). The geometry and material properties of the specimens were listed in Table 1. The FE analysis was useful to broaden the study and provide more validation samples for the theoretical study.

The developed FE model was shown in Fig. 2(b). As shown in Fig. 2, the bottom of two modular columns were pin-constrained and out-of-plane displacement of the web of the ceiling beam was constrained to simulate the lateral restraint apparatus. The frame and the infill corrugated steel panel were meshed independently with a mesh size of 40 mm, as displayed in Fig. 2(b). This mesh strategy was adopted to avoid irregular elements and improve the solving efficiency. All members including the frame column, frame beam and infill corrugated steel panel were modeled by the four-node shell element S4R with reduced integration. The bilinear model was used for steel with the elastic modulus,
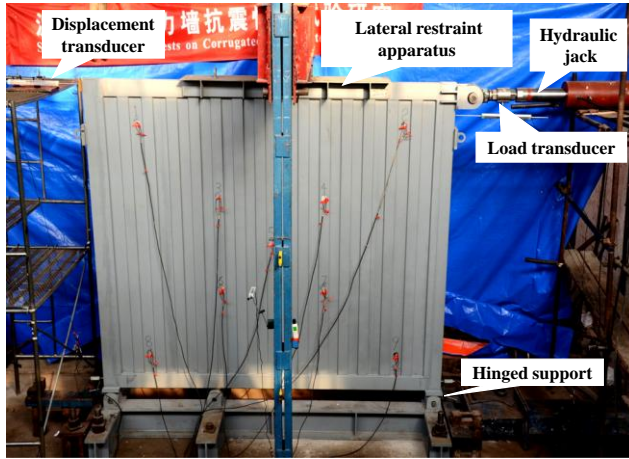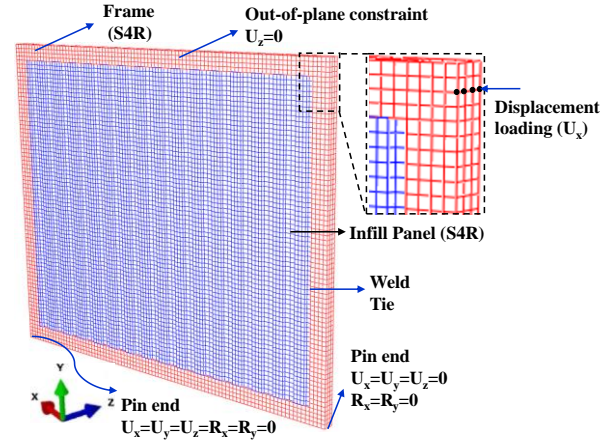
(a) Test setup   (b) FE model

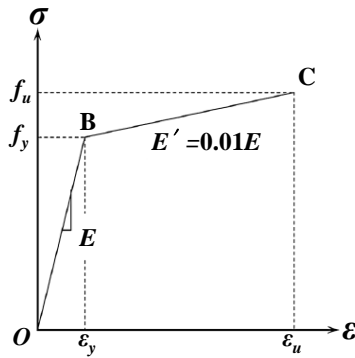Fig. 2 Test setup and FE model for CSPSW
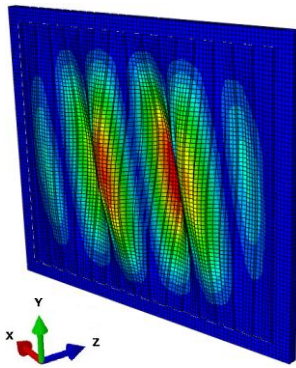

Fig. 3 Stress-strain curves for steel in the FEM

Fig. 4 First buckling mode of CSPSW

yield strength, ultimate strength and ultimate strain given in the reference (Ding *et al*. 2018), as shown in Fig. 3. The hardening modulus was taken as 1/100 times elastic modulus and the Poisson's ratio was taken as 0.3.

The initial geometric imperfection was considered in the FE model. Linear elastic eigenvalue buckling analyses were firstly performed using the subspace iteration method in ABAQUS to extract the buckling modes, as shown in Fig. 4. The geometric imperfection amplitude was taken as $H/200$ times of the first buckling mode, where H was the height of infill corrugated steel panel (Eurocode 2003,

Bahrebar *et al*. 2016). Displacement load the same as the loading program of the tests was then applied at one end of the ceiling beam. The loading history of the specimens was generally based on the ATC-24 (1992) guidelines for cyclic testing of structural steel components. The yield displacement Δ_y was defined as the displacement corresponding to the yield load F_y, which was equal to $0.7F_u$ approximately, where F_u was the ultimate load according to the test results. The elastic cycles were conducted at displacement levels of $0.25\Delta_y$, $0.50\Delta_y$, $0.70\Delta_y$ and inelastic cycles were then taken at Δ_y, $1.5\Delta_y$, $2\Delta_y$, $3.0\Delta_y$, $5\Delta_y$, $7\Delta_y$, $8\Delta_y$.

2.2 Validation of the FE model

The horizontal force versus the displacement hysteretic curves obtained by the FE analysis and tests were compared in Fig. 5. Generally, the numerical results agreed well with the test results. The numerical results almost coincided with the test data in the elastic stage. Further, the FE model can simulate well the transitory decline of force in the buckling stage and the increasing of force in the post-buckling stage. It indicates the effectiveness of the FE model on simulating the seismic behavior of CSPSWs. The elastic-plastic inter-story drift ratio is stipulated as 0.02rad for multi-layer and high-rise steel structures in Chinese code for seismic design of buildings (GB 50011-2010 2010). The failure inter-story drift ratios of the specimens range from 0.0207rad to 0.0275rad, demonstrating the satisfactory deformation capacity of CSPSWs.

The initial stiffness (K_0) and ultimate load (F_u) of the FE analysis and tests were listed in Table 2. The initial stiffness K_0 was defined as the initial scant stiffness of the skeleton curve, as shown in Fig. 5(a). It indicates that the FE model averagely overestimate the elastic stiffness of CSPSWs with FE-to-test ratio ranging from 0.85 to 1.19. The mean value and coefficient of variation (COV) of the FE-to-test rations are 1.05 and 0.11, respectively. The slight overestimation may be caused by the difference of boundary condition between the FE model and test apparatus. There is a gap between the lateral restraint apparatus and specimen for

(a) Specimen CSPSW-1

(b) Specimen CSPSW-2

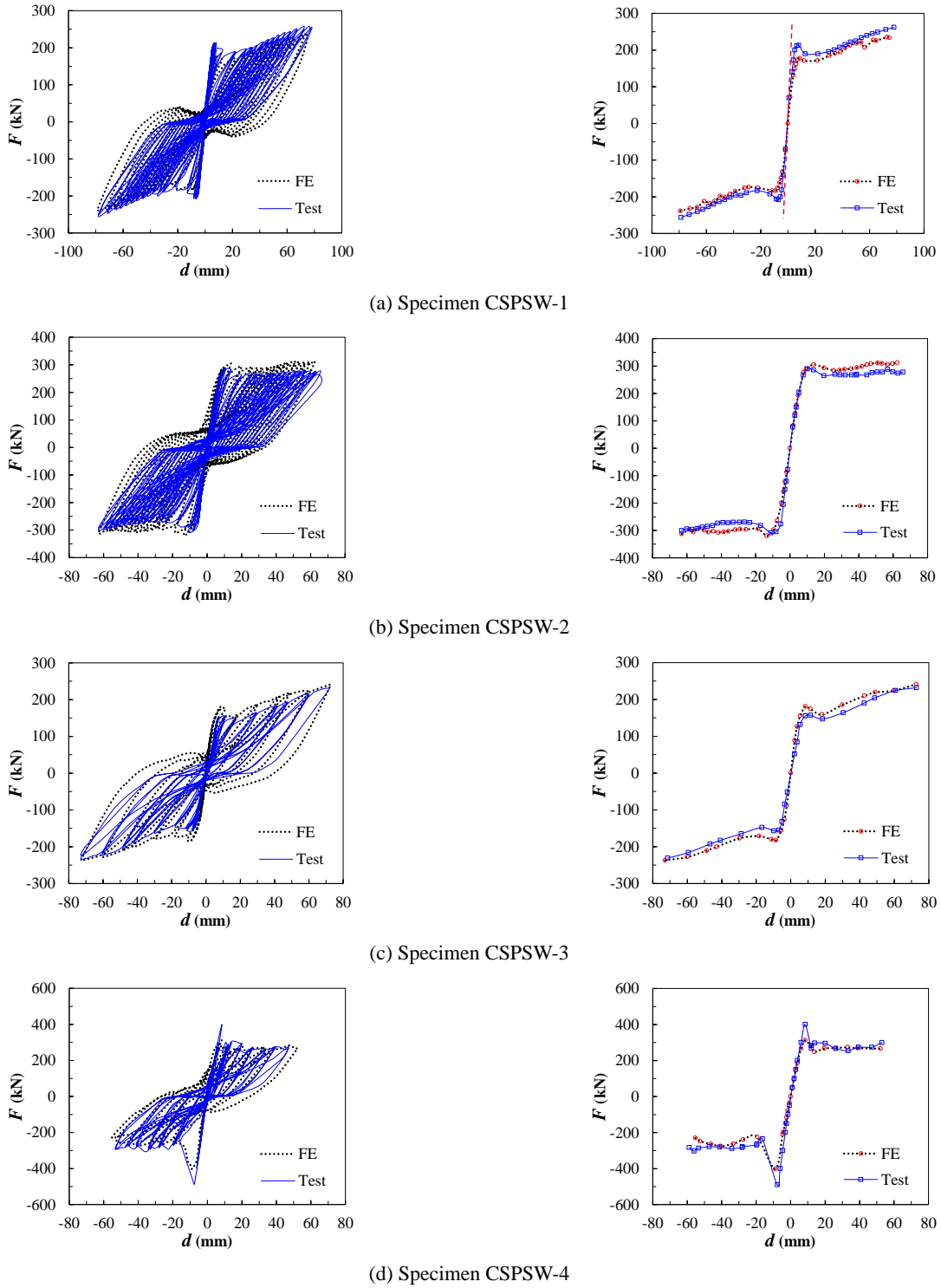(c) Specimen CSPSW-3

(d) Specimen CSPSW-4

Fig. 5 Comparisons of hysteretic and skeleton curves between tests and FE predictions

installation, as shown in Fig. 2(a). However, the lateral restraint of the ceiling beam is ideal and stronger than the tests. The comparisons in Table 2 also show that the FE model can well predict the ultimate load of CSPSWs with the mean value and COV of the FE-to-test rations to be 1.05 and 0.11, respectively. The FE results of failure modes are also agreeable to the test ones, as shown in Figs. 6. The above comparisons further verify the accuracy and reasonableness of the FE model.

3. Theoretical derivation

3.1 General

To provide a universal calculation method of initial stiffness of CSPSWs, the theoretical derivation was conducted in this section. Fig. 7 shows the analytical model developed in this paper. The initial stiffness of the CSPSW, K_0, consists of the stiffness of the outer frame, K_f, the

Table 2 Validation of the FE model

Specimen	Loading direction	K_0 (kN/mm)			F_u (kN)		
		Test	FE	FE/Test	Test	FE	FE/Test
CSPSW-1	+	38.9	46.2	1.19	287	235	0.82
	−	41.2	46.5	1.13	283	239	0.84
CSPSW-2	+	52.0	54.4	1.05	289	312	1.08
	−	55.7	54.5	0.98	308	320	1.04
CSPSW-3	+	23.2	27.6	1.19	213	241	1.13
	−	29.8	27.6	0.93	218	237	1.09
CSPSW-4	+	52.6	56.9	1.08	400	312	0.78
	−	66.7	56.9	0.85	487	403	0.83
Mean	-	-	-	1.05	-	-	0.95
COV	-	-	-	0.11	-	-	0.15

(a) Specimen CSPSW-1   (b) Specimen CSPSW-3
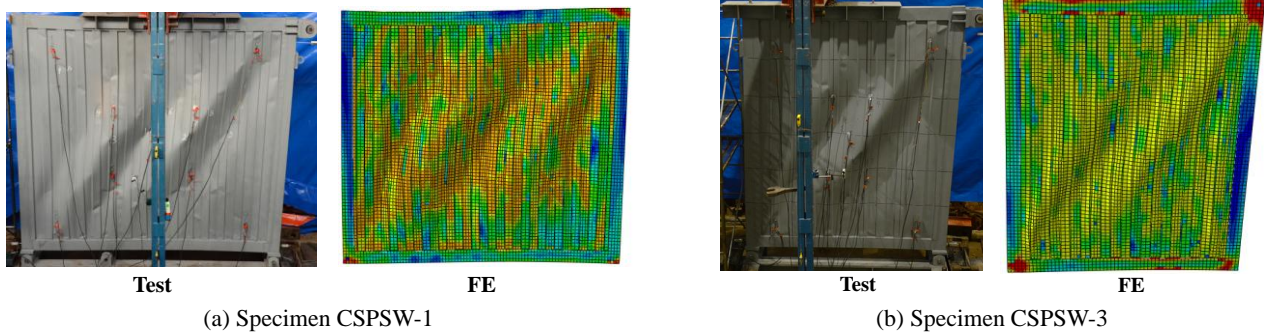
Fig. 6 Comparisons of failure mode between tests and FE simulation
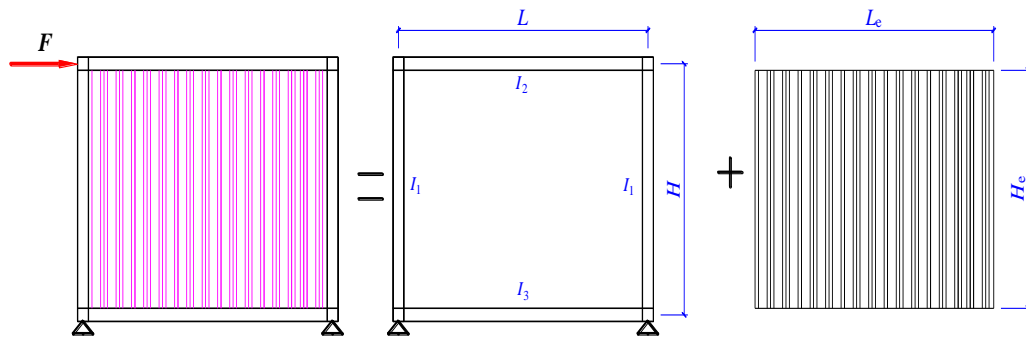
Fig. 7 Schematic diagram of initial stiffness of CSPSW

(a) Moment diagram under design load   (b) Moment diagram under unit load
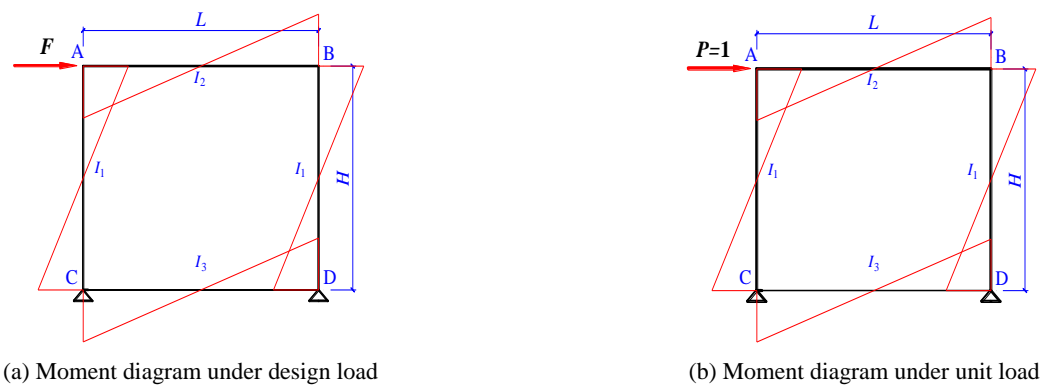
Fig. 8 Lateral displacement calculation of the frame by the unit-load method

stiffness of the infill corrugated steel panel, K_w, i.e.

$$K_0 = K_f + K_w \qquad (1)$$

The outer frame was pin-constrained at the bottom of the modular column, simulating the typical boundary condition of the module unit (Ding *et al.* 2017). The stiffness of the outer frame and infill panel were derived based on structural mechanics, respectively (Liu and Zhang 2006).

3.2 Initial stiffness of the frame

The moment diagram of the frame under design load F and unit load $P = 1$ were shown in Fig. 8, where L and H denotes the length and height of the module, respectively, I_1, I_2, and I_3 denote the second moment of area of the modular column, the ceiling beam and the floor beam, respectively. The lateral displacement of the frame under design load F was given by

$$\Delta_f = \int \frac{M_p \cdot \overline{M}}{EI} d_s \qquad (2)$$

where, M_p and $\overline{M}$ denote the moment of the member under design load and unit load, respectively, and E means the elastic modulus of the steel.

To solve the statically indeterminate structure, the linear stiffness ratio of the ceiling beam (k_1) and floor beam (k_2) to the modular column can be calculated as follows

$$k_1 = \frac{H}{L} \cdot \frac{I_2}{I_1} \qquad (3)$$

$$k_2 = \frac{H}{L} \cdot \frac{I_3}{I_1} \qquad (4)$$

In addition, the following dimensionless parameters μ, ϕ were defined to simplify the expression of the moment.

$$\mu = \frac{k_1}{k_2} + 6k_1 + 1 \qquad (5)$$

$$\phi = \frac{k_1}{\mu \cdot k_2}(1 + 3k_2) \qquad (6)$$

The force method was implemented to solve the moment of the frame under design load F, as given in Eqs. (7)~(8).

$$M_A = M_B = \phi \frac{F \cdot H}{2} \qquad (7)$$

$$M_C = M_D = (1 - \phi)\frac{F \cdot H}{2} \qquad (8)$$

where, M_A, M_B, M_C, and M_D represent the moment at the

corresponding corner of the frame, as indicated in Fig. 8.

Similarly, the moment of the frame under unit load P can be determined by the following equations.

$$\overline{M_A} = \overline{M_B} = \phi \frac{H}{2} \qquad (9)$$

$$\overline{M_C} = \overline{M_D} = (1 - \phi)\frac{H}{2} \qquad (10)$$

The stiffness of the frame was defined as the ratio of the design load F to the lateral displacement Δ_f, i.e.

$$K_f = \frac{F}{\Delta_f} \qquad (11)$$

Substituting Eqs. (2)~(10) into Eq. (11) yields the initial stiffness of the frame, as expressed in Eq. (12).

$$K_f = \frac{1}{\frac{H^3}{6E_1I_1}(3\phi^2 - 3\phi + 1) + \frac{LH^2\phi^2}{12E_2I_2} + \frac{(1-\phi)^2H^2L}{12E_3I_3}} \qquad (12)$$

3.3 Initial stiffness of the infill corrugated steel panel

The infill corrugated steel panel subjected to moment and shear force under horizontal force. The moment diagram and shear diagram of the infill panel under design load F and unit load $P = 1$ were illustrated in Figs. 9(a) and (b), respectively. The lateral displacement of the infill panel under design load Δ_w was given as follows.

$$\Delta_w = \int \frac{M_p \cdot \overline{M}}{EI_z} d_s + \int k \frac{V_p \cdot \overline{V}}{GA_e} d_s \qquad (13)$$

where, M_p and V_p denote the moment and shear force under design load, respectively. $\overline{M}$ and $\overline{V}$ denote the moment and shear force under unit load, respectively. I_z and A_e denote the second moment of area and effective shear section area of the infill panel, respectively. G denotes the shear modulus of the steel, which can be determined by the elastic modulus, E, and the Poisson's ratio, v, i.e.

$$G = \frac{E}{2(1 + v)} \qquad (14)$$

k denotes the nonuniform coefficient of shear stress, which can be determined by Eq. (15) (Liu and Zhang 2006). For the trapezoidally corrugated steel plate, the plate was folded by several rectangular plate strips. Theoretically, the nonuniform coefficient of shear stress was taken as 1.2.

$$k = \frac{A}{I^2}\int_A \frac{S^2}{b^2}dA \qquad (15)$$

where, A denotes the area of the section, S denotes the first

(a) Moment diagram and shear diagram under design load

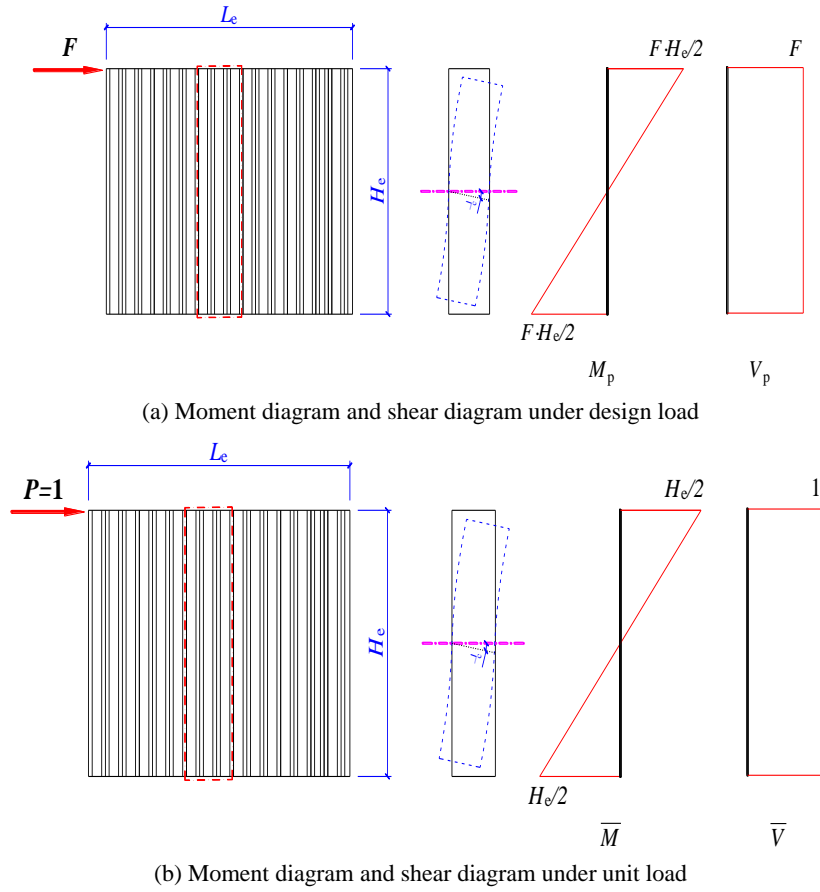(b) Moment diagram and shear diagram under unit load

Fig. 9 Lateral displacement calculation of the infill panel by the unit-load method

moment of area of the section, I denotes the second moment of area of the section and b denotes the width of the section.

Fig. 10 shows the cross section characteristics of the corrugated steel plate. The inclined ladder section was decomposed to the horizontal direction and vertical direction. Thus, the second moment of area of the section can be determined as follows

$$I_z = \frac{1}{12} t \cdot L_e^3 + h \cdot t \sum d_i^2 \qquad (16)$$

where, L_e denotes the net length of the infill panel, as shown in Fig. 9. t denotes the thickness of the panel and h denotes the height of the crest. d_i denotes the distance of the ith ladder to the midline of the section.

The effective shear section area of the infill panel can be calculated as follows

$$A_e = \eta \cdot L_e \cdot t \qquad (17)$$

where, η is the shape factor of the section, indicating the ratio between the unfolding length and the net length of the corrugated steel plate, i.e.

$$\eta = \frac{a+d+c}{a+b+c} \qquad (18)$$

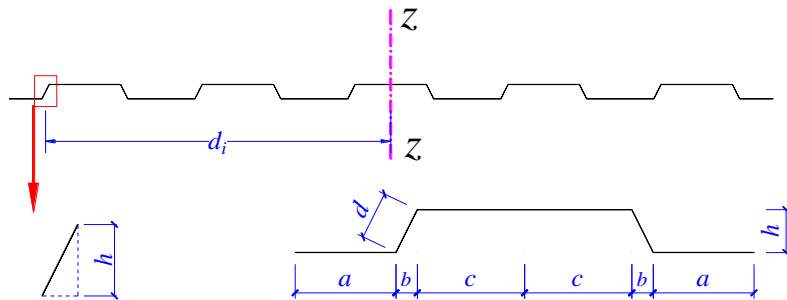where, a, b, c, d denote the parameters of the corrugated steel plate, as shown in Fig. 10.

Fig. 10 Cross section characteristics of the corrugated steel plate

(a) Frame (WBK1~WBK4)   (b) CSPSW (YBK1~YBK4)
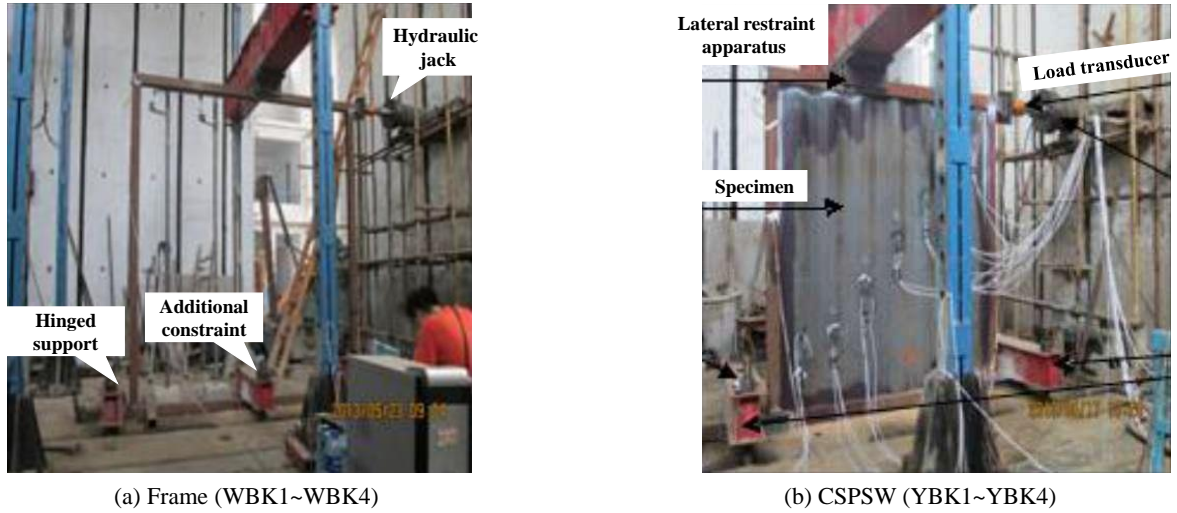
Fig. 11 Test setup (Liu 2013)

The reduction of initial stiffness caused by elastic buckling and geometrical imperfection is given by the following equation (JGJ/T 380-2015 2015).

$$\gamma = 0.014 \ln(L_e / H_e) - 0.118 \ln(\lambda) + 1.24 \qquad (19)$$

where, L_e and H_e denote the effective length and height of the infill panel. λ denotes the relative height-to-thickness ratio of the infill panel, which can be expressed as

$$\lambda = \frac{H_e}{t \cdot \sqrt{\dfrac{235}{f_y}}} \qquad (20)$$

The initial stiffness of the infill corrugated steel panel can be determined as follows

$$K_w = \frac{F}{\Delta_w} \qquad (21)$$

Then, Eq. (22) is gained by substituting Eqs. (13)~(20) into Eq. (21).

$$K_w = \frac{\gamma}{\dfrac{H_e^3}{12E \cdot I_z} + \dfrac{3.12 \cdot H_e}{E \cdot \eta \cdot L_e \cdot t}} \qquad (22)$$
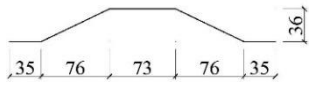
Substituting Eq. (12) and Eq. (22) into Eq. (1) yields the initial stiffness of CSPSWs, i.e.

$$K_0 = \frac{1}{\dfrac{H^3}{6E_1 I_1}(3\phi^2 - 3\phi + 1) + \dfrac{LH^2\phi^2}{12E_2 I_2} + \dfrac{(1-\phi)^2 H^2 L}{12E_3 I_3} + \dfrac{\gamma}{\dfrac{H_e^3}{12E \cdot I_z} + \dfrac{3.12 \cdot H_e}{E \cdot \eta \cdot L_e \cdot t}}} \qquad (23)$$

3.4 Validation of the theoretical formulas

The tests conducted by Ding *et al*. (2018) and Liu (2013) were unitized to validate the theoretical formulas. Meanwhile, the developed FE model was used to provide more samples. Specimen WBK1~WBK4 denote the four frame specimens tested by Liu (2013), which can be used to validate the theoretical formulas for the stiffness of the frame, i.e., Eq. (12). The schematic view of the test setup was shown in Fig. 11. The specimens were tested under monotonic lateral force to failure. The geometry and material properties of the specimens were listed in Table 3. Specimen CSPSW1~CSPSW4 denote the cyclic tests conducted by Ding *et al*. (2018). CSPSW1-0.8~CSPSW4-3.2 denote the numerical results obtained by the established FE model in this paper. The name of the specimen is constituted by the test specimen (CSPSW1~CSPSW4) and

Table 3 The geometry and material properties of the specimens (Liu 2013)

Type	Section (mm)	t^* (mm)	E^* (Gpa)	f_y^* (MPa)	f_u^* (MPa)
Corrugated steel plate	35, 76, 73, 76, 35 / 36 Specimen YBK1~YBK4	1.6 Specimen YBK1~YBK4	204	346	448
Frame beam/ Frame column	□100×100×4	4.0	204	299	420

*t: thickness of the steel plate; *E: elastic modulus; *f_y: yield strength; *f_u: ultimate tensile strength

the thickness of the infill panel (0.8 mm, 2.4 mm and 3.2 mm). Take Specimen CSPSW1-0.8 for example, the thickness of infill panel is 0.8 mm and the other geometrical sizes are the same as the test Specimen CSPSW1. The Technical Specification for Steel Plate Shear Walls (JGJ/T 380-2015 2015) was also adopted for comparison. The theoretical formula provided in JGJ/T 380-2015 was given as follows.

$$K_0 = \frac{\gamma \cdot E \cdot t}{\dfrac{1}{(L_e / H_e)^3} + \dfrac{3.12}{L_e / H_e}} \tag{24}$$

The comparisons between the theoretical values (K_0) and the related test and FE results were listed in Table 4 and shown in Fig. 12. The symbol "+" means the positive loading and "−" means the negative loading, respectively. In Fig. 2(a), the push (from right to left) is defined as positive loading and the pull (from left to right) is defined as negative loading. The comparisons indicate that Eq. (12) can predict well the initial stiffness of frame with K_0-to-test ranging from 0.73 to 0.98. The additional constraint was applied on the bottom beam of the Specimen WBK3 and WBK4 (Fig. 11(a)) during the test, leading to the underestimation of the initial stiffness. Moreover, the initial stiffness of the frame used for the fabrication of Specimen CSPSW1~CSPSW4 was 0.80 kN/mm according to the numerical simulation and the theoretical results was 0.81 kN/mm by Eq. (12), validating the accuracy of Eq. (12) further. Therefore, Eq. (12) was verified and can be used to calculate the stiffness of modules when the corrugated steel plate was removed for building function. The Eq. (23)

Table 4 Validation of the theoretical formulas against the tests and FE analysis

| Specimen		$L \times H$ (m×m)	$L_e \times H_e$ (mom)	Test (kN/mm)	JGJ/T 380-2015		This paper	
					K_0 (kN/mm)	K_0/ Test	K_0 (kN/mm)	K_0/ Test
WBK1		1.1×1.1	1.0×1.0	4.44	-	-	4.33	0.98
WBK2		2.1×2.1	2.0×2.0	0.70	-	-	0.62	0.89
WBK3		3.1×3.1	3.0×3.0	0.22	-	-	0.19	0.86
WBK4		4.1×4.1	4.0×4.0	0.11	-	-	0.08	0.73
YBK1		1.1×1.1	1.0×1.0	48.7	36.1	0.74	43.7	0.90
YBK2		2.1×2.1	2.0×2.0	36.4	29.6	0.81	32.9	0.90
YBK3		3.1×3.1	3.0×3.0	40.3	25.4	0.63	34.8	0.86
YBK4		4.1×4.1	4.0×4.0	25.9	23.1	0.89	25.4	0.98
CSPSW1	+	3.6×3.0	3.3×2.7	38.9	33.2	0.85	40.7	1.05
	−	3.6×3.0	3.3×2.7	41.2	33.2	0.81	40.7	0.99
CSPSW2	+	3.6×3.0	3.3×2.7	52.0	47.4	0.91	56.1	1.07
	−	3.6×3.0	3.3×2.7	55.7	47.4	0.85	56.1	1.01
CSPSW3	+	2.5×3.0	2.2×2.7	23.2	18.1	0.78	22.3	0.96
	−	2.5×3.0	2.2×2.7	29.8	18.1	0.61	22.3	0.75
CSPSW4	+	3.6×3.0	3.3×2.7	52.6	33.2	0.63	48.5	0.92
	−	3.6×3.0	3.3×2.7	66.7	33.2	0.50	48.5	0.73
Specimen		$L \times H$ (m×m)	$L_e \times H_e$ (m×m)	FE (kN/mm)	JGJ/T 380-2015		This paper	
					K_0 (kN/mm)	K_0/ FE	K_0 (kN/mm)	K_0/ FE
CSPSW1-0.8		3.6×3.0	3.3×2.7	25.3	15.4	0.61	27.3	1.08
CSPSW1-2.4		3.6×3.0	3.3×2.7	66.4	57.3	0.86	60.2	0.91
CSPSW1-3.2		3.6×3.0	3.3×2.7	96.1	79.9	0.83	81.5	0.85
CSPSW3-0.8		2.5×3.0	2.2×2.7	14.6	8.20	0.56	15.7	1.08
CSPSW3-2.4		2.5×3.0	2.2×2.7	36.4	33.6	0.92	37.4	1.03
CSPSW3-3.2		2.5×3.0	2.2×2.7	52.6	42.5	0.81	48.8	0.93
CSPSW4-0.8		3.6×3.0	3.3×2.7	25.0	15.4	0.62	28.5	1.14
CSPSW4-2.4		3.6×3.0	3.3×2.7	64.8	57.3	0.88	63.2	0.98
CSPSW4-3.2		3.6×3.0	3.3×2.7	93.7	79.9	0.85	86.3	0.92
Mean		-	-	-	-	0.76	-	0.94
COV		-	-	-	-	0.17	-	0.11

(a) Frame
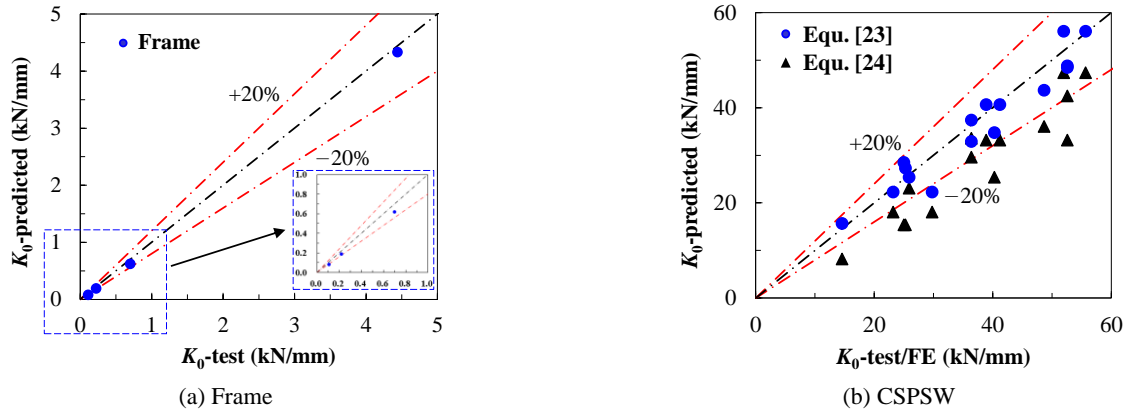
(b) CSPSW

Fig. 12 Validation of the theoretical formulas

derived in this paper was verified to be effective to predicted the stiffness of CSPSWs with the K_0-to-test and K_0-to-FE ratio ranging from 0.73 to 1.14 with a mean value of 0.94 and COV of 0.11. It should be mentioned that there was a gap with a width of 10 mm between the lateral restraint apparatus and specimen in Fig. 2(a) for convenience of installing of the specimens. Therefore, a slight global twist occurred when the push force was applied on the specimens, leading to a lower initial stiffness than negative loading. It can be found that the K_0-to-test ratios in positive direction were higher than that of negative direction and Eq. (23) underestimated the initial stiffness in negative direction slightly. However, the theoretical formulas provided in JGJ/T 380-2015 underestimated the initial stiffness of CSPSWs with the K_0-to-test and K_0-to-FE ratio ranging from 0.50 to 0.92 with a mean value of 0.76 and COV of 0.17. The formulas in JGJ/T 380-2015 neglect the contribution of the corrugation effect to the initial stiffness of CSPSWs, leading to the underestimation. These comparisons verify the effectiveness and accuracy of the theoretical formulas proposed in this paper, which will be used for parametric analysis in the following section.

3.5 Limitation and discussion

The height-to-thickness ratio should be less than or equal to 600 to ensure the out-of-plane stiffness of steel plate shear walls and avoid the overlarge initial imperfection, i.e., Eq. (25), as required by Technical Specification for Steel Plate Shear Walls (JGJ/T 380-2015 2015). Accordingly, Eq. (26) was recommended for CSPSWs according to the equivalence of out-of-plane stiffness.

$$\frac{H_e}{t} \cdot \sqrt{\frac{f_y}{235}} \le 600 \tag{25}$$

$$\frac{H_e}{\left(\left(3\eta - 2\sqrt{\frac{b^2 + h^2}{(a+b+c)^2}}\right) \cdot th^2\right)^{\frac{1}{3}}} \cdot \sqrt{\frac{f_y}{235}} \le 600 \tag{26}$$

4. Parametric analysis

4.1 General

The proposed theoretical formulas has been validated and used for parametric analysis to provide a better comprehensive of the initial stiffness of CSPSWs. The parameters considered in this study include the length of the CSPSW (L), the height of the CSPSW (H), the thickness of the CSPSW (t), and the height of the crest of the corrugated steel plate (h). The summary of the parameters were listed in Table 5.

4.2 Length of the infill corrugated steel panel

The length of the infill corrugated steel panel varies from 2 m to 10 m with a step of 1 m. Figs. 13(a), (b) and (c) show the initial stiffness of CSPSWs (K) with different length of infill panel and constant t, constant H and constant h, respectively. It is shown that the initial stiffness increases almost linearly with the increasing of the length of the infill panel and the slope increases with the increasing of t, H and h. Take $t = 0.8$ mm for example, the initial stiffness

Table 5 Summary of the parameters in parametric study

Parameter	Values
L	2 m, 3 m, 4 m, 5 m, 6 m, 7 m, 8 m, 9 m, 10 m
H	2.6 m, 2.7 m, 2.8 m, 2.9 m, 3.0 m, 3.1 m, 3.2 m, 3.3 m, 3.4 m
t	0.8 mm, 1.2 mm, 1.6 mm, 2.0 mm, 2.4 mm, 2.8 mm, 3.2 mm, 3.6 mm, 4.0 mm
h	0 mm, 10 mm, 20 mm, 30 mm, 40 mm, 50 mm, 60 mm, 70 mm, 80 mm

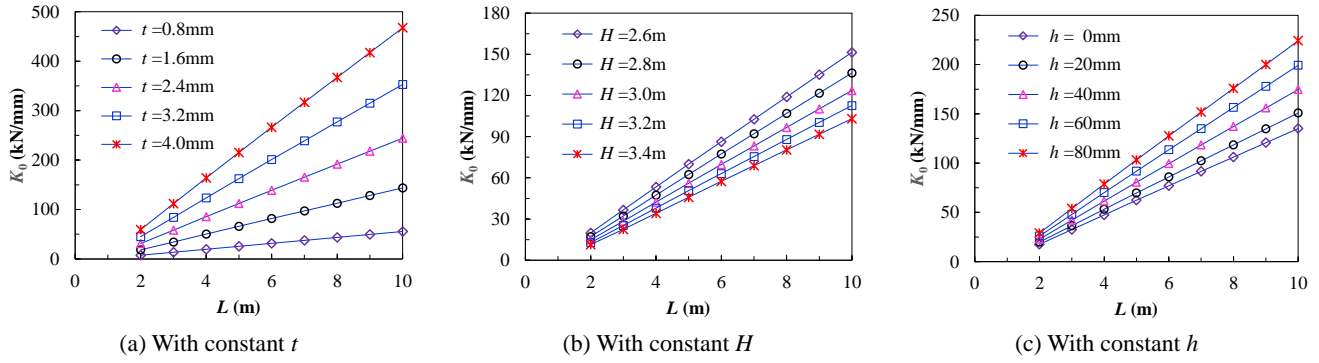(a) With constant *t*   (b) With constant *H*   (c) With constant *h*

Fig. 13 Influence of length of the infill corrugated steel panel on initial stiffness of CSPSW

(a) With constant *t*   (b) With constant *L*   (c) With constant *h*
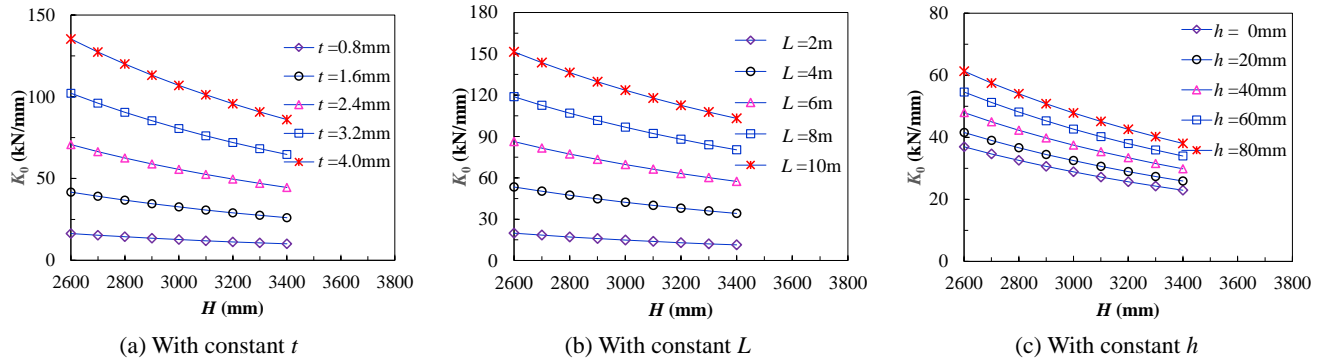
Fig. 14 Influence of height of the infill corrugated steel panel on initial stiffness of CSPSW

(a) With constant *L*   (b) With constant *H*   (c) With constant *h*
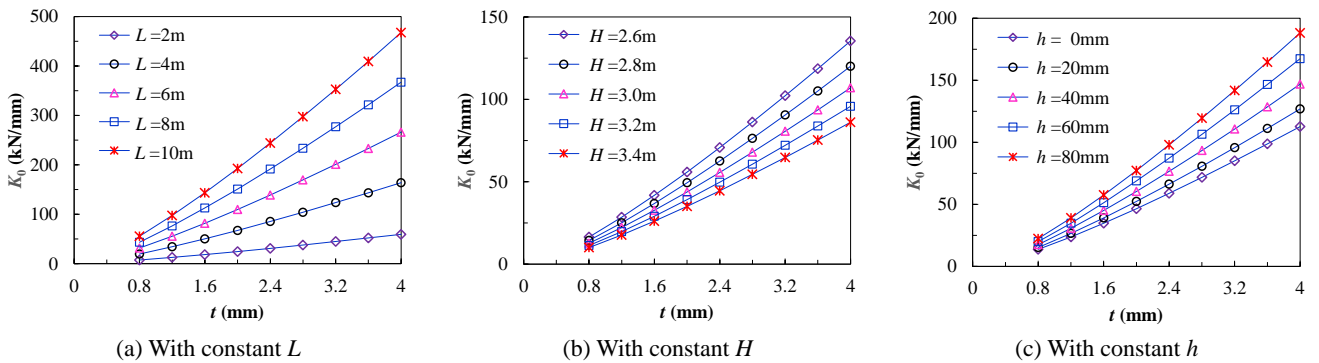
Fig. 15 Influence of thickness of the infill corrugated steel panel on initial stiffness of CSPSW

increases from 7.5 kN/mm to 55.6 kN/mm as the length of the infill panel increases from 2 m to 10 m.

4.3 Height of the infill corrugated steel panel

The height of the infill corrugated steel panel varies from 2.6 m to 3.4 m with a step of 0.1 m. The variation of initial stiffness as the height of the infill panel varies are shown in Fig. 14. It can be seen that the initial stiffness decreases with the increasing of *H*. The slope decreases with the decreasing of *t*, *L* and *h*. The initial stiffness remains almost constant when *t* = 0.8 mm and *L* = 2 m. The initial stiffness decreases rapidly with higher *t*, *L* and *h*. For instance, the initial stiffness decreases by 36.4% from 135.3 kN/mm to 86.0 kN/mm as height of the height of the infill panel increases from 2.6 m to 3.4 m.

4.4 Thickness of the infill corrugated steel panel

The thickness of the infill corrugated steel panel varies from 0.8 mm to 4.0 mm with a step of 0.4 mm. Fig. 15 shows the variation of initial stiffness with the increasing of *t*. It's obvious the initial stiffness increases rapidly with the increasing of *t* and the slope increases with increasing of *L*, *H* and *h*. For example, the initial stiffness increases by 4.4 times from 55.6 kNmm to 467.5 kN/mm as the thickness of the corrugated steel panel increases from 0.8 mm to 4.0 mm. It indicates that the initial stiffness of CSPSW is significantly affected by the thickness of the infill panel.

4.5 Crest height of the infill corrugated steel panel

The crest height of the infill corrugated steel panel

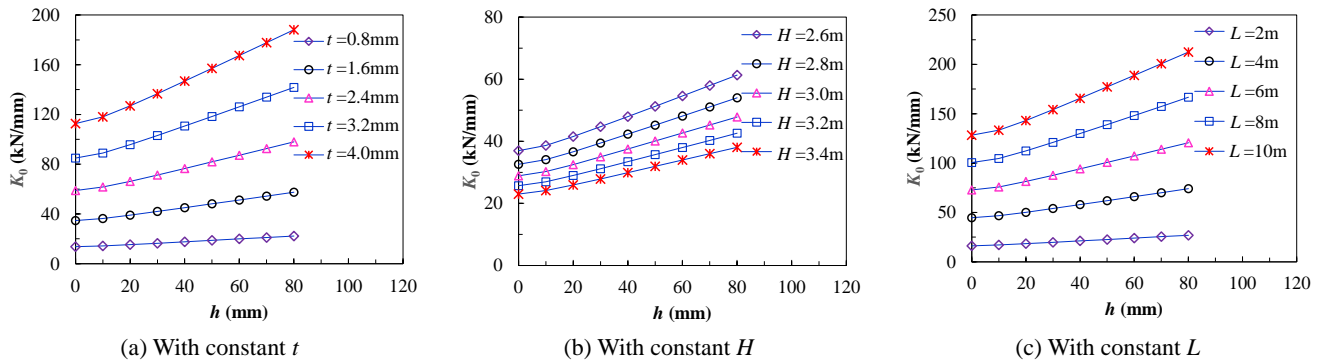(a) With constant *t*   (b) With constant *H*   (c) With constant *L*

Fig. 16 Influence of crest height of the infill corrugated steel panel on initial stiffness of CSPSW

varies from 0 mm to 80 m with a step of 10 mm. It should be mentioned that $h = 0$ mm denotes the infill panel is unstiffened steel plate. The initial stiffness of CSPSWs with increasing h are shown in Fig. 16. It indicates that the initial stiffness increases with the increasing of crest height. The slope increases with the increasing of t, H and L. Compared to the unstiffened steel plate, the effect of the corrugation is obvious, especially with higher t and L. For instance, the initial stiffness increases by 70% from 112.6 kN/mm to 188.1 kN/mm as the crest height increases from 0 mm to 80 mm. It implies that it is effective to improve the initial stiffness of CSPSW by increasing the crest height of the corrugated steel panel. It's noteworthy that length and height of the infill panel are usually depend on the building function design of the building. Therefore, it is recommended to adjust the initial stiffness of CSPSWs by changing the thickness or the crest height of the corrugated steel plate.

5. Conclusions

This paper focuses on the initial stiffness of CSPSWs in modular steel construction through numerical and theoretical study. An elaborate FE model that considered geometrical and material nonlinearity was developed to provide detailed simulation of seismic performance CSPSWs. The accuracy of the FE model was verified by the cyclic tests conducted by Ding *et al*. (2018). Then, the theoretical formulas predicting the initial stiffness of CSPSWs were derived and validated. Parametric analysis was also conducted based on the developed calculation method to reveal the influence of the geometrical parameters on the initial stiffness of CSPSWs. The main conclusions are drawn as follows.

- The developed FE model is useful to simulate seismic performance of CSPSWs, including the initial stiffness, shear capacity and failure mode.
- Compared to recommended design formulas in JGJ/T 380-2015, the derived theoretical formulas in this paper take the corrugation effect into consideration. The accuracy of the theoretical formulas has been verified by the related tests and numerical results. It can be used for the design of CSPSWs in modular steel construction.

- The corrugation effect on initial stiffness of CSPSWs is obvious, especially with higher length and thickness of the infill panel. It may be over-conservative and uneconomical neglecting the contribution of the corrugation on the initial stiffness of CSPSWs.
- Parametric analysis indicates that the length, the height, the thickness and the crest height of the infill corrugated steel panel influence the initial stiffness of CSPSWs obviously. The initial stiffness of CSPSWs increases by increasing the length of the infill panel, decreasing the height of the infill panel, increasing the thickness of the infill panel or increasing the crest height of the infill panel. It's recommended to change the initial stiffness of CSPSWs by adjusting the thickness or the crest height of the infill corrugated steel panel.

References

ABAQUS (2013), User manual Version 6.13; DS SIMULIA Corp., Providence, RI, USA.
ATC-24 (1992), Guidelines for Cyclic Seismic Testing of Components of Steel Structures; Applied Technology Council, Redwood City, CA, USA.
Bagherinejad, M.H. and Haghollahi, A. (2018), "Topology optimization of steel plate shear walls in the moment frames", *Steel Compos. Struct*., *Int. J*., **29**(6), 771-783. https://doi.org/10.12989/scs.2018.29.6.771
Bahrebar, M., Kabir, M.Z., Zirakian, T., Hajsadeghi, M. and Lim, J.P.B. (2016), "Structural performance assessment of trapezoidally-corrugated and centrally-perforated plate shear walls", *J. Constr. Steel Res*., **122**, 584-594. https://doi.org/10.1016/j.jcsr.2016.03.030

Barakat, S. and Leblouba, M. (2018), "Experimental and analytical study on the shear strength of corrugated web steel beams", *Steel Compos. Struct., Int. J.*, **28**(2), 251-266. https://doi.org/10.12989/scs.2018.28.2.251

Deng, E.F., Yan, J.B., Ding, Y., Zong, L., Li, Z.X. and Dai, X.M. (2017), "Analytical and numerical studies on steel columns with novel connections in modular construction", *Int. J. Steel Struct.*, **17**(4), 1613-1626. https://doi.org/10.1007/s13296-017-1226-5

Deng, E.F., Zong, L., Ding, Y., Dai, X.M., Lou, N. and Chen, Y. (2018a), "Monotonic and cyclic response of bolted connections with welded cover plate for modular steel construction", *Eng. Struct.*, **167**, 407-419. https://doi.org/10.1016/j.engstruct.2018.04.028

Deng, E.F., Zong, L., Ding, Y. and Luo, Y.B. (2018b), "Seismic behavior and design of cruciform bolted module-to-module connection with various reinforcing details", *Thin-Wall. Struct.*, **133**, 106-119. https://doi.org/10.1016/j.tws.2018.09.033

Ding, Y., Deng, E.F., Zong, L., Dai, X.M., Lou, N. and Chen, Y. (2017), "Cyclic tests on corrugated steel plate shear walls with openings in modularized-construction", *J. Constr. Steel Res.*, **138**, 675-691. https://doi.org/10.1016/j.jcsr.2017.08.019

Ding, Y., Deng, E.F., Zong, L., Dai, X.M., Lou, N. and Chen, Y. (2018), "Experimental study on seismic performance of corrugated steel plate shear wall in modular steel construction", *J. Build. Eng.*, **39**(12), 110-118. https://doi.org/10.14006/j.jzjgxb.2018.12.013

Emami, F., Mofid, M. and Vafai, A. (2013), "Experimental study on cyclic behavior of trapezoidally corrugated steel shear walls", *Eng. Struct.*, **48**, 750-762. https://doi.org/10.1016/j.engstruct.2012.11.028

Eurocode (2003), Design of Steel Structures; Part 1.5: Plated Structural elements, European Committee for Standardization; Brussels, Belgium.

Farnsworth, D. (2014), "Modular tall building design at Atlantic Yards B2", *Proceedings of CTBUH 2014 international conference*, Shanghai, China, pp. 492-499.

Farzampour, A., Laman, J.A. and Mofid, M. (2015), "Behavior prediction of corrugated steel plate shear walls with openings", *J. Constr. Steel Res.*, **114**, 258-268. https://doi.org/10.1016/j.jcsr.2015.07.018

Giriunas, K., Sezen, H. and Dupaix, R.B. (2012), "Evaluation, modelling, and analysis of shipping container building structures", *Eng. Struct.*, **43**, 48-57. https://doi.org/10.1016/j.engstruct.2012.05.001

GB 50011-2010 (2010), Code for seismic design of buildings. China Architecture & Building Press, Beijing, China.

JGJ/T 380-2015 (2015), Technical Specification for Steel Plate Shear Walls; China Architecture & Building Press, Beijing, China.

Kim, J.Y. and Lee, J.K. (2014), "A basic study on the application of modular construction", *J. Korean Hou. Asso.*, **25**(4), 39-46. https://doi.org/10.6107/JKHA.2014.25.4.039

Lawson, R.M., Ray, O. and Chris, G. (2014), *Design in Modular Construction*, CRC Press, Boca Raton, FL, USA.

Liu, Y. (2013), "Experimental research on shear and wind resistance of container house siding", Master Dissertation; Tianjin University, Tianjin, China.

Liu, S.P. and Zhang, Y.M. (2016), *Structural Mechanics*, Tianjin University Press, Tianjin, China.

Luo, R., and Edlund, B. (1996), "Shear capacity of plate girders with trapezoidally corrugated webs", *Thin-Wall. Strcut.*, **26**(1), 19-44. https://doi.org/10.1016/0263-8231(96)00006-7

Park, H.K. and Ock, J.H. (2015), "Unit modular in-fill construction method for high-rise buildings", *KSCE J. Civ. Eng.*, **20**(4), 1201-1210. https://doi.org/10.1007/s12205-015-0198-2

Park, K.S., Moon, J.H., Lee S.S., Bae K.W. and Roeder, C.W. (2016), "Embedded steel column-to-foundation connection for a modular structural system", *Eng. Struct.*, **110**, 244-257. https://doi.org/10.1016/j.engstruct.2015.11.034

Qiu, J., Zhao, Q.H., Yu, C. and Li, Z.X. (2018), "Experimental Studies on Cyclic Behavior of Corrugated Steel Plate Shear Walls", *J. Struct. Eng.*, **144**(11), p. 04018200. https://doi.org/10.1061/(ASCE)ST.1943-541X.0002165

Tong, J.Z. and Guo, Y.L. (2015), "Elastic buckling behaviour of steel trapezoidal corrugated shear walls with vertical stiffeners", *Thin-Wall. Struct.*, **95**, 31-39. https://doi.org/10.1016/j.tws.2015.06.005

Yu, Y.J. and Chen, Z.H. (2018), "Rigidity of corrugated plate sidewalls and its effect on the modular structural design", *Eng. Struct.*, **175**, 191-200. https://doi.org/10.1016/j.engstruct.2018.08.039

Zuo, Y. and Zha, X.X. (2017), "FEM and experimental study on mechanical property of container building with holes", *Int. J. Steel Struct.*, **17**(1), 175-194. https://doi.org/10.1007/s13296-015-0132-y

BU